Astron. Astrophys. 316, 350–354 (1996)

ASTRONOMY
AND
ASTROPHYSICS

Variation of electron-strahl width in the high-speed solar wind: Ulysses observations

C.M. Hammond[1], **W.C. Feldman**[2], **D.J. McComas**[2], **J.L. Phillips**[2], **and R.J. Forsyth**[3]

[1] SRI International, AEOL 409-47, 333 Ravenswood Avenue, Menlo Park, CA 94025, USA
[2] Los Alamos National Laboratory, MS D466, Los Alamos, NM 87545, USA
[3] The Blackett Laboratory, Imperial College, London

Received 19 February 1996 / Accepted 15 July 1996

Abstract. Halo electron velocity distributions have been surveyed during the first full Ulysses southern polar pass from January 1994 through April 1995. The data examined range from approximately 50° S heliolatitude to the maximum poleward extent of the Ulysses orbit, approximately 80° S, and then back through the solar equator to 35° N heliolatitude. During this traversal the radial distance of Ulysses ranged from 3.8 to 1.3 AU, allowing the same heliolatitude to be sampled at two different distances. The angular width of the electron strahl is found to be broader throughout the coronal hole region than that reported for high speed streams by in-ecliptic spacecraft during the mid 1970's. The average strahl width (full width at half maximum) extrapolated to 1 AU is found to be 49° for 77 eV electrons. The strahl width broadens substantially between 1.3 and 2.3 AU after which the width is approximately constant. The broadening is greatest for the lower energy (77 eV) electrons. One might expect a broadening of the strahl if scattering dominates magnetic focusing of electrons caused by the decreasing magnetic field magnitude with increasing solar distance. The results presented here suggest that substantial wave-particle scattering of the electron strahl occurs, consistent with interpretations of the reduction in electron heat flux with increasing heliocentric distance measured by Ulysses.

Key words: solar wind

1. Introduction

Solar wind electron velocity distributions may be divided into 3 components: a thermal portion of the distribution termed the "core", the "halo" or suprathermal background present at all pitch angles, and the sharply field aligned portion of the suprathermal electrons termed the "strahl" (Feldman et al. 1975; Rosenbauer et al. 1977; Pilipp et al. 1987a). The strahl consists of those halo electrons whose energies are great enough to allow them to escape the electrostatic potential of the Sun. Characteristics of the strahl have been presented by Pilipp et al. (1987b, 1990). As these strahl particles move away from the Sun outside its potential well scattering collisions become sufficiently infrequent that both their energy and magnetic moment are conserved. The conservation of these two quantities yields a distribution of suprathermal electrons that is focused along the magnetic field (Schulz and Eviatar 1972). Broadening of this distribution in pitch angle is the result of binary Coulomb collisions or some wave-particle scattering mechanism. In this work we examine the pitch angle distribution of the strahl and how it varies with heliocentric distance and heliographic latitude using data from the plasma instruments onboard the Ulysses spacecraft.

Previous missions have relied on the tilt of the heliospheric current sheet to probe high heliomagnetic latitudes. Feldman et al. (1978) showed that the strahl in the high speed solar wind (and thus at higher magnetic latitude) is more narrow than in the low speed solar wind, which generally originates at lower latitudes. These observations were taken in the ecliptic plane near 1 AU. The Ulysses mission made measurements at heliocentric distances up to 5.4 AU and at latitudes up to $\pm 80.2°$. In this paper we present a subset of these measurements from 1.3 to 3.8 AU and latitudes up to $-80°$. These measurements were made while Ulysses was continuously within the high speed solar wind of the south-polar coronal hole. The average solar wind speed during this interval was 770 km/s with minimum and maximum speeds of 660 and 859 km/s, respectively. Because solar wind flow conditions throughout this interval were generally very uniform and independent of latitude, we are able to determine the radial variation of strahl in the coronal hole. We will show that there is substantial broadening of the strahl in the high speed solar wind between 1.3 and 2.3 AU. We propose a possible mechanism that explains this in terms of scattering by unique features prevalent at high heliolatitudes and large heliocentric distances.

Send offprint requests to: C.M. Hammond

2. Data

The electron measurements are from the electron plasma instrument onboard Ulysses (Bame et al. 1992). This instrument returns both two and three dimensional measurements of electron velocity distributions between 0.86 eV to 814 eV; only three dimensional spectra were utilized in this study. The average angular width of the instrument in the meridianal direction is approximately 21° while in the azimuthal direction the angular width is 11.25° or 22.5° depending on the mode. Most of the data were collected when the angular width in the azimuthal direction was 11.25°. The solar wind velocity was measured with the ion plasma instrument which returns three dimensional velocity space measurements. Pitch angle measurements were determined using 64 sec resolution magnetic field data (Balogh et al. 1992).

We characterized the strahl at various energies in terms of its width in pitch angle space through a range of heliolatitudes and radial distances. Electrons with energies in the solar wind rest frame between 70–90, 106–124, 149–175, and 207–243 eV were examined for this purpose. At the lower energies these bins are slightly different than the instrument's energy bins since the energy binning is made in the solar wind rest frame. We refer to these energy bins as energies of 77, 115, 162, and 225 eV, respectively. The data used in this study were not continuous. Instead eleven weeks of data were chosen to give representative measurements over a wide range of distances and heliolatitudes and radial distances between 1.3 to 3.8 AU. The eleven intervals were chosen randomly based only on the basis of coverage in radial distance and heliolatitude. During this time the spacecraft traveled from a heliolatitude of 49° S in January 1994 to a peak Southerly latitude of 80.2° in September of 1994. The peak Northerly latitude included in this study is 35° degrees, reached by Ulysses in April of 1995.

Several steps were involved in reducing the data to characterize the strahl widths. For a given electron energy the electron measurements were first transformed into the solar wind proton rest frame. The pitch angle of each measurement was then determined using the average magnetic field measured in the sampling interval. The data were rotated such that the peak measurement always occurred at pitch angles less than 90°. Thus, in our data examples 0° pitch angle is always the direction along the field line away from the sun. Using 64 second resolution field data there were typically three measurements of the magnetic field in the sampling interval. If the angle between any of these vectors was greater than 10° the entire electron scan was rejected. Additionally, individual electron measurements for a given pitch angle with less than 5 counts were rejected. Data contaminated by sunlight-induced backgrounds were eliminated from the final pitch-angle distributions. To improve statistics the data were mirrored about 0° pitch angle and binned into 15°-wide pitch angle bins. For clarity we will often refer to both positive and negative pitch angles. However, it should be remembered that because of the mirroring of the data, positive and negative pitch angles are not statistically independent.

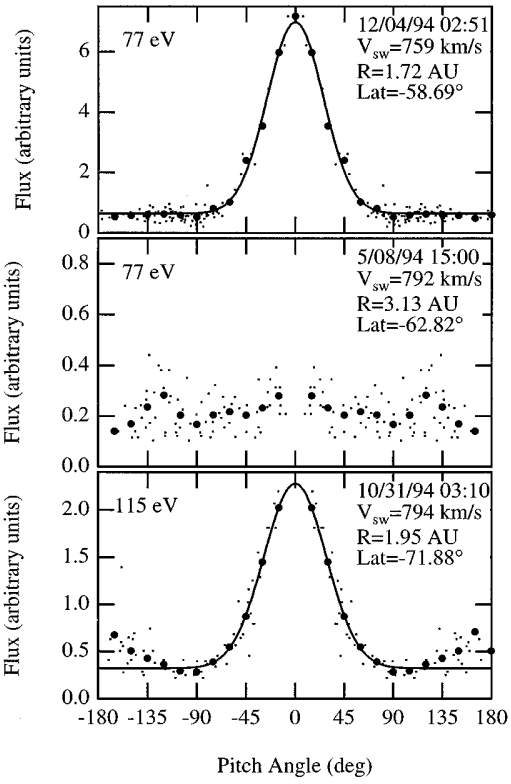

Fig. 1. Three representative pitch angle distributions seen in the high speed solar wind. Top two panels show 77 eV electrons while the bottom panel is 115 eV electrons. Dots are the measured data and filled circles are these data binned into 15° wide pitch angle bins. The solid line is the Gaussian fit to the data

Some representative electron pitch-angle distributions are shown in Fig. 1. The top two panels are for 77 eV electrons while the bottom panel is for 115 eV electrons. All three panels, however, are representative of the types of distributions found at all four of the energies examined in this study. Many times the strahl peak is well resolved as in the top panel of Fig. 1. At other times the strahl appears to be absent, lacking a clearly resolved peak as in the middle panel. Less often, a small counter-streaming component is seen, as in the lower panel. This particular example of a counter-streaming component is not indicative of a CME in which the sunward (lower panel near ±180°) and antisunward (lower panel near 0°) fluxes are usually more nearly comparable.

Only those data which have a clearly defined peak such as that shown in the top and bottom panels of Fig. 1, are fit. An automated fitting routine performed Gaussian fits of strahl spectra meeting certain criteria:

1. At least one binned data point located inclusively within ±15° pitch angle.
2. Peak signal to background ratio > 2.
3. Peak measurement must be located within ±45° pitch angle.
4. If available, the data point at 0° (±15°) pitch angle must be greater than 80% of the data point at ±15° (±30°) pitch angle.

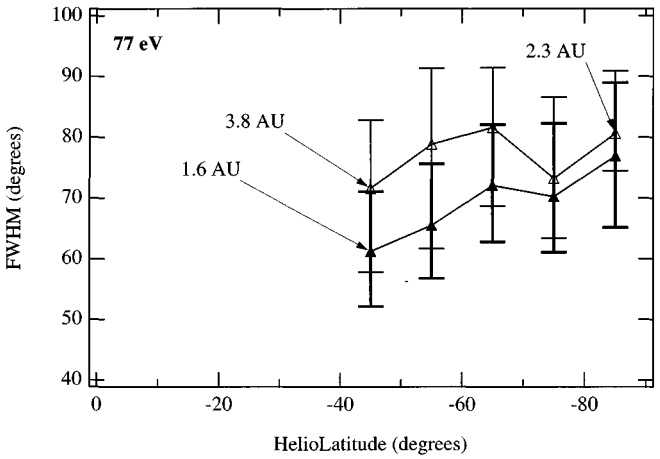

Fig. 2. Median full width at half maximum of the strahl for 77 eV electrons in 10° wide heliolatitude bins. Error bars show the upper and lower quartiles of the distribution of measurements in each latitude bin. Unfilled triangles with thin error bars are for the inbound pass while filled triangles with thick error bars are from the outbound pass

These criteria prevent fits of intervals where the strahl was not present or when lack of data coverage prevented the strahl from being seen. The last statement assures that the distribution is very roughly a gaussian distribution.

Before fitting the spectra the peak of each pitch-angle distribution, background (halo component) measurement was calculated by averaging the binned data points located at pitch angles of $\pm 75°$, $\pm 90°$, and $\pm 105°$. A nonlinear minimization routine was then used to fit the binned spectra for the four different energy channels to a Gaussian distribution of the following form:

$$j(\alpha) = K_0 + K_1 \exp\left(-\frac{\alpha^2}{K_3^2}\right) \quad (1)$$

where j is the flux as a function of pitch angle, α, and K_0 is the halo background calculated as described above. Each pitch-angle spectrum was assumed to have the strahl centered at 0° pitch angle. The parameter K_3 determines the width of the distribution and is related to the full width at half maximum as: FWHM = $2\sqrt{\ln 2}K_3$.

3. Observations

Over the time interval examined, Ulysses covered a wide range of both heliographic latitudes and radial distances. Figure 2 shows the median width of the strahl (FWHM) for the 77 eV electrons versus heliolatitude. The data have been binned separately for the south-going and north-going portions of the southern polar pass. This enables the combined effects of radial distance and latitude on the strahl to be examined. The figure shows that at each given latitude the width of the strahl increases with increasing radial distance. We therefore conclude that radial distance rather than latitude primarily determines the width.

Figure 3 shows the same 77 eV electron data binned by radial distance using bins of 0.2 AU width. Also shown are the

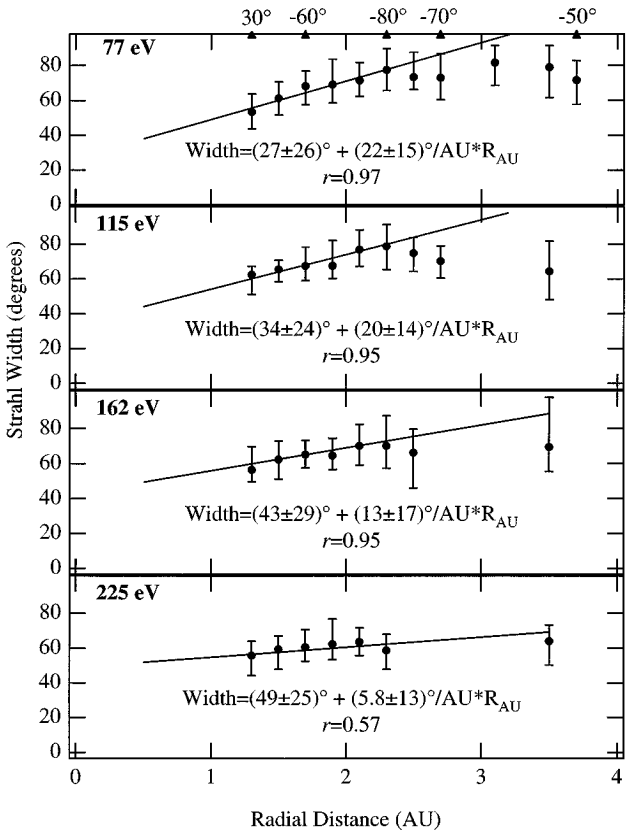

Fig. 3. Medians of FWHM of the strahl in 0.2 AU radial distance bins for 77, 115, 162, and 225 eV electrons. Error bars show the upper and lower quartiles of the distribution of measurements in each bin. Linear fit and correlation coefficient, r, are shown on each panel

distribution widths for 115, 162, and 225 eV electrons. At the higher energies, the counts were often too small to resolve the strahl peak. In these cases no fits could be done and thus some of the bins at higher energies are empty. The error bars shown for each data point of Fig. 3 are the upper and lower quartiles of the distribution of points in each bin. Note that the separation between upper and lower quartiles is often greater than 20° indicating that when the strahl is present its width can vary over a large range.

Most clear from Fig. 3 is the trend toward increasing strahl width with increasing radial distance. A maximum width occurs at about 2.3 AU, beyond the width stays approximately constant. The same general trend is seen in all four energy channels. A linear fit of the variation between 1.3 and 2.3 AU is shown for each energy. For all but the highest energy electrons the correlation coefficient, r, is quite high for the variation within 2.3 AU. Note that the slopes of the linear fit decrease with increasing energy. The confidence intervals on the slopes, however, are large. A more detailed look at the variation of slope with energy will be presented in the discussion section.

4. Discussion and conclusions

For the 77 eV electrons there is some indication that the widths begin to decrease beyond 3 AU. This may be a latitudinal effect. At 3.5 AU, Ulysses was located at −55° S at Carrington longitudes between 285° to 24°. This region includes the longitude range between 250° and 350°, shown to have an increased compressional component (McComas et al. 1995). The average FWHM for the 77 eV electrons between 250° and 350° is 74° compared to 92° for the points at the same radial distance and latitude outside this longitude range. If the compressional structures observed by McComas et al. result from the propagation of a compressional wave from lower latitudes, we would expect to detect higher strahl widths within this range of Carrington longitudes. The opposite effect was observed. We therefore conclude that because both average widths are equal within their individual ranges of variation, that compressional effects on the widths of electron strahls is insignificant.

The strahl widths presented here are much broader than the 1 AU observations of Feldman et al. (1978). Extrapolated to 1 AU we find the FWHM of the 77 eV electron strahl to be 49° compared to the 25.5° (37.8°) FWHM for 86 (62) eV electrons observed by Feldman et al. Furthermore, for a given radial distance the median values of the FWHM shown here do not exhibit the strong energy dependence seen by Feldman et al. (1977). The Feldman et al. data sampled high heliomagnetic latitudes by relying on the tilt of the heliospheric current sheet to bring the spacecraft into the high speed wind of the coronal hole. These intervals were specially chosen to be particularly clean examples of the high speed wind. In contrast, in the present study we have chosen our intervals randomly, selecting them only on the basis of coverage in radial distance and heliolatitude. We have seen in Fig. 1 that the strahl is variable in the high speed wind. The relatively large difference in the upper and lower quartiles in Fig. 3 also indicate that the strahl width is variable. We suggest that a possible explanation for this discrepancy is due to this variability in the strahl although longer term variability of the strahl caused by solar cycle effects cannot be ruled out.

Figure 3 appears to show that the strahl width increases with increasing radial distance. This result runs counter to predictions based on exospheric theory as augmented by Coulomb collisions (Lemons & Feldman 1983). However, the error bars show that there is a wide range of variation in the strahl width within a given radial distance bin. In order to better quantify the range of possible slopes we perform a Monte Carlo analysis of the possible slopes. Using data only within the region of increasing strahl width up to and including 2.3 AU, we randomly pick a value for each radial distance bin between the upper and lower quartiles. We fit these data using linear least squares and record the slope. We repeat the experiment picking new random samples 300,000 times. Such a technique assumes the data is equally likely to be anywhere in the range given by the error bars rather than being distributed normally about the median value. The results from this analysis are shown as a plot of slope versus energy in Figure 4. The error bars shown on each point are the 68% confidence intervals from the distribution of slopes created

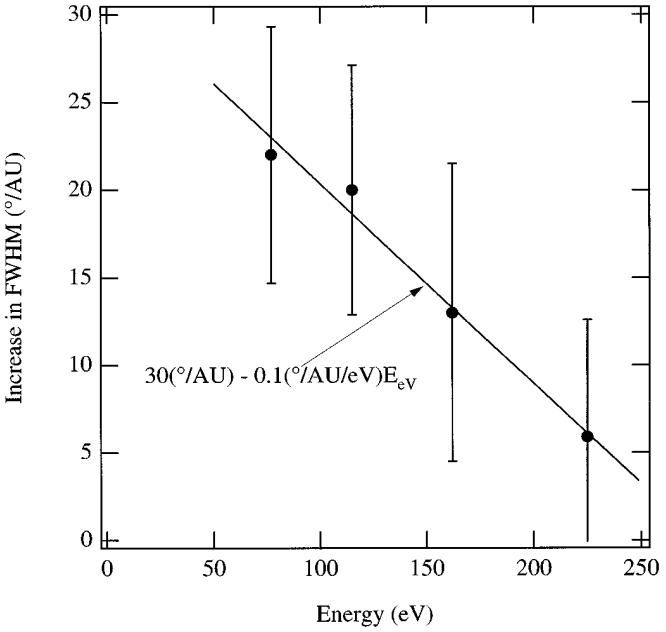

Fig. 4. Slope of the increase in strahl width with radial distances versus electron energy. Error bars are 68% confidence intervals as described in the text

in the Monte Carlo analysis. The amount of scattering decreases with increasing energy and thus it cannot be said with statistical certainty that the slopes of the higher energy electrons are positive. However, the figure suggests that for the lower energy electrons the change in strahl width with distance is positive. This result runs counter to that predicted by exospheric theory invoking just binary coulomb collisions. (e.g., Feldman et al. 1978; Lemons & Feldman 1983).

At radial distances less than 2.3 AU the amount of scattering appears to be a function of radial distance rather than heliolatitude. The broadening of the strahl will cause a decrease in the heat flux. The lack of a heliolatitude effect is in agreement with the results of Scime et al. (1995) who showed that there is little evidence for a variation of electron heat flux with heliolatitude once the radial variation has been removed. Although there is some evidence of a heliolatitude dependence at large radial distances with the data that have been examined in this study, the effect is sufficiently small that no conclusions may be drawn.

Figure 4 also suggests that the scattering process is energy dependent. Whereas the radial gradient of strahl widths at the lower energies is high, that at the highest electron energy (225 eV) is low: little or no change in the strahl width is observed with increasing radial distance. The results of a linear fit to these points is shown in the figure. The correlation coefficient of this fit showing the trend toward less scattering at higher energies is 0.99. With only four data points the result is not conclusive, however, the figure does suggest that the broadening of the strahl decreases with increasing energy.

As the strahl moves out into the decreasing magnetic field one would expect a focusing of the strahl instead of the observed broadening indicating some scattering mechanism other

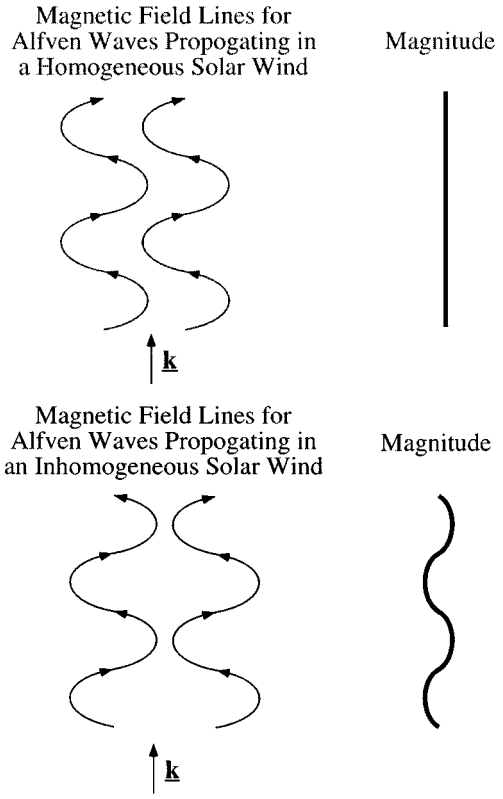

Fig. 5. Schematic showing the production of time variable mirrors by Alfvén waves traveling in an inhomogeneous medium

than that due to binary Coulomb interactions must be present. Lemons & Feldman (1983) have shown that even accounting for binary Coulomb collisions, exospheric theory under predicts the strahl width in high speed streams. Thus the scattering may be due to wave-particle interactions. Gary et al. (1994) have proposed the whistler heat flux mechanism to explain the heat flux gradient observed in the ecliptic by Scime et al. (1994). It is tempting to explain the broadening seen above the ecliptic with this same mechanism. However, for the whistler heat flux instability to flourish $T_\perp/T_\parallel$ must be greater than approximately 1 (Gary et al. 1994). This condition is not easily met for the suprathermal electrons in the high latitude solar wind. In Fig. 5 we sketch a possible mechanism which would allow the whistler heat flux instability to scatter the strahl in the high speed solar wind. Alfvén waves propagating in an inhomogeneous medium can form temporary magnetic mirrors as sketched in the figure. Such Alfvénic fluctuations have been observed in the high speed solar wind (Balogh et al. 1995). These mirrors will broaden the strahl locally, however, this broadening is not permanent since as the strahl moves away from the mirror then it returns to its original width. Inside the mirror where the strahl has a large perpendicular velocity, the criteria for the whistler heat flux instability may be satisfied. The triggering of the whistler heat flux instability would then permanently broaden the strahl.

In summary, we have shown that the electron strahl is scattered, thereby increasing its angular width between radial distances of 1.3 to 2.3 AU. The amount of scattering increases with decreasing electron energy. We have proposed a scattering mechanism that could possibly explain this effect. It consists of a two step process in which magnetic mirrors formed by Alfvén waves propagating in an inhomogeneous medium increase the perpendicular velocity of the strahl sufficiently for the whistler heat flux instability to be triggered leading to the angular scattering of strahl electrons. We have described this mechanism only schematically and it may not be unique. A more quantitative analysis of scattering mechanisms must be done before the cause of the strahl broadening will be certain.

Acknowledgements. We thank A. Balogh for the magnetic field data. Work at Los Alamos was performed under the auspices of the U.S. Department of Energy with financial support from NASA.

References

Balogh A., Beek T.J., Forsyth R.J., Hedgecock P.C., Marquedan R.J., Smith E.J., Southwood D.J., Tsurutani B.T., 1992, A&AS 92, 221

Balogh A., Smith E.J., Tsurutani B.T., Southwood D.J., Forsyth R.J., Horbury T.S., 1995, Science 268, 1007

Bame S.J., McComas D.J., Barraclough B.L., Phillips J.L., Sofaly K.J., Chavez J.C., Goldstein B.E., Sakurai R.K., 1992, A&AS 92, 237

Feldman W.C., Asbridge J.R., Bame S.J., Montgomery M.D., Gary S.P., 1975, J. Geophys. Res. 80, 4181

Feldman W.C., Asbridge J.R., Bame S.J., Gosling J.T., Lemons D.S., 1978, J. Geophys. Res. 83, 5285

Gary S.P., Scime E.E., Phillips J.L., Feldman W.C., 1994, J. Geophys. Res. 99, 23391

Lemons D.S., Feldman W.C., 1983, J. Geophys. Res. 88, 6881

McComas D.J., Barraclough B.L., Gosling J.T., Hammond C.M., Phillips J.L., Neugebauer M., Balogh A., Forsyth R.J., 1995, J. Geophys. Res. 100, 19893

Pilipp W.G., Miggenrieder H., Montgomery M.D., Mühlhäuser K.-H., Rosenbauer H., Schwenn R., 1987a, J. Geophys. Res. 92, A2, 1075

Pilipp W.G., Miggenrieder H., Montgomery M.D., Mühlhäuser K.-H., Rosenbauer H., Schwenn R., 1987b, J. Geophys. Res. 92, A2, 1093

Pilipp W.G., Miggenrieder H., Mühlhäuser K.-H., Rosenbauer H., Schwenn R., 1987, J. Geophys. Res. 95, A5, 6305

Rosenbauer H., Schwenn R., Marsch E., Meyer B., Miggenrieder H., Montgomery M.D., Mühlhäuser K.-H., Pilipp W., Voges W., Zink S.M., 1977, J. of Geophys. 42, 561

Schulz M., Eviatar A., 1972, Cosmic Electrodynamics 2, 402

Scime E.E., Bame S.J., Feldman W.C., Gary S.P., Phillips J.L., Balogh A., 1994, J. Geophys. Res. 99, 23401

Scime E.E., Bame S.J., Phillips J.L., Balogh A., 1995, Space Sci. Rev. 72, 105